J Nanostruct 12(2): 389-404, Spring 2022

RESEARCH PAPER

# Fabrication of pH-Sensitive Dual Antibiotic-Loaded PVP-PEG@ZnO Nanohybrids for Controlled Drug Release to Combat Bacteria

*Mohammad Mazloum-Ardakani [1]*, Azra Ebadi [1], Zahra Tavangar [2], Fereshteh Vajhadin [1], Reza Behjatmanesh-Ardakani [3], Seyed Mohammad Moshtaghioun [4], and Reihaneh Haghniaz [5]*

[1] *Department of Chemistry, Faculty of Science, Yazd University, Yazd, Iran*

[2] *Department of Physical Chemistry, Faculty of Chemistry, University of Kashan, Iran*

[3] *Department of Chemistry, Faculty of Sciences, Payame Noor University (PNU), Ardakan, Iran*

[4] *Department of Biology, Faculty of Science, Yazd University, Yazd, Iran*

[5] *University of California, Los Angeles Terasaki institute for biomedical, USA*

## ARTICLE INFO

***Article History:***
*Received 29 January 2022*
*Accepted 27 March 2022*
*Published 01 April 2022*

***Keywords:***
*Antibacterial*
*Drug release kinetics*
*Sol-gel*
*Theoretical calculations*
*Zinc oxide nanohybrid*

## ABSTRACT

The increasing rate of antibiotic resistance is a major threat for healthcare systems that elevate the necessity of exploring new materials to combat infectious diseases. Zinc oxide-based nanomaterials have emerged as promising candidates to minimize drug resistance due to their potential antibacterial properties and also as cargo to deliver antibiotics for sustained release. Here, we engineer zinc oxide-based colloidal hybrid system comprised of poly (ethylene glycol) (PEG) and amphiphilic poly (vinyl pyrrolidone) (PVP) as a stabilizing agent for controlled drug release. Ciprofloxacin (CF) and metronidazole (MZ) with different polarities are encapsulated in PVP-PEG@ZnO nanohybrid as model antibiotics against aerobic and anaerobic bacteria. The present study investigates the effects of the CF/MZ: ZnO nanohybrid composition ratio on encapsulation efficiency, drug release, and antimicrobial activity. For the comparison, we also synthesized PEG@ZnO incorporated enrofloxacin (EFX) (model hydrophobic drug) by a sol-gel procedure. We report that our in vitro drug release kinetics are well aligned with Ritger-Peppas and Sahlin-Peppas equations. The binding efficacy of drugs and PVP-PEG@ZnO nanohybrid was investigated using molecular dynamic simulations and DFT methods. Free energy calculations and root-mean-square deviation (RMSD) were applied to analyze binding interactions. This research will provides an insight into the engineering of ZnO-based nanomaterials for dual-drug delivery to improve infection treatment.

**How to cite this article**
*Mazloum-Ardakani M, Ebadi A, Tavangar Z, Vajhadin F, Behjatmanesh-Ardakani R, Moshtaghioun S M, Haghniaze R. Fabrication of pH-Sensitive Dual Antibiotic-Loaded PVP-PEG@ZnO Nanohybrids for Controlled Drug Release to Combat Bacteria J Nanostruct, 2022; 12(2):389-404. DOI: 10.22052/JNS.2022.02.015*

## INTRODUCTION

Infectious diseases kill over 17 million people annually due to the reduced clinical effectiveness of current treatments resulting from drug resistance. Development of new materials for the treatment of patients with antibiotic-resistant infections is a challenging task. Recent advances in biomaterials have provided a variety

* *Corresponding Author Email: mazloum@yazd.ac.ir*

of materials such as organic (polymeric micelles and surfactants) and inorganic (silica and metallic nanoparticles) or hybrid materials (organic and inorganic) for effective drug delivery [1-4]. Among inorganic nanoparticles, metallic oxide nanostructures, especially nano-scale ZnO, have gained significant importance in biomedical fields, particularly as biocidal and purifying agents due to the production of reactive oxygen species (ROS) that damage bacterial cells. ZnO nanoparticles have already been used as antimicrobial agents showing remarkable resistance against various bacterial pathogens [5]. Furthermore, zinc has a significant role in glucose metabolism and acts as an enzyme activator that helps in insulin secretion [6].

Drug encapsulation into a nanocargo is an effective technique that protects the active substance against degradation and controls the drug release in vitro and in vivo. It also reduces the limitation of conventional formulation such as side effects and unsuitable bioavailability [7-9]. The co-encapsulation of multiple drugs and active therapeutic substances in a single delivery system is a promising approach to provide advanced infection therapies [10, 11]. Simultaneous encapsulation of drugs with different polarities and solubilities in nanoparticles holds the potential to improve the effectiveness of treatment with the benefit of a synergistic drug effect through sustained combinatorial drug release. Several studies have examined the co-encapsulation of multiple drugs into a single cargo, including nanocarrier based on bio-polymer coated graphene oxide [12], silica nanoparticles composite [13], multilayered microparticles [14], and poly(D,L-lactide-co-glycolide) (PLGA) nanoparticles [15]. The correct combination of drugs can better adjust cell signaling to raise the healthcare effect and decrease drug resistance [16, 17]. There is an increasing need to develop new approaches that lead to effective antibacterial therapies to overcome antibacterial resistance sustainably.

In this study, ZnO nanoparticles incorporated -ciprofloxacin (CF) and metronidazole (MZ) - were fabricated in polymeric solution using the cost-effective and low-temperature approach in an aqueous solution by sol-gel and co-precipitation method. These polymeric nanoparticles were developed with the goal of co-delivering of CF and MZ. CF is a fluoroquinolone with broad activity against Gram-positive and Gram-negative aerobic organisms but has no activity against anaerobic bacteria. MZ is particularly effective in treating infections from susceptible anaerobic bacteria and parasites [18]. Both the CF and MZ belong to the class of quinolone and nitroimidazole that inhibit DNA-directed cell wall biosynthesis. Herein, we took advantage of the synergistic effects of CF and MZ to fight against a broad spectrum of bacteria while simultaneously addressing antibacterial

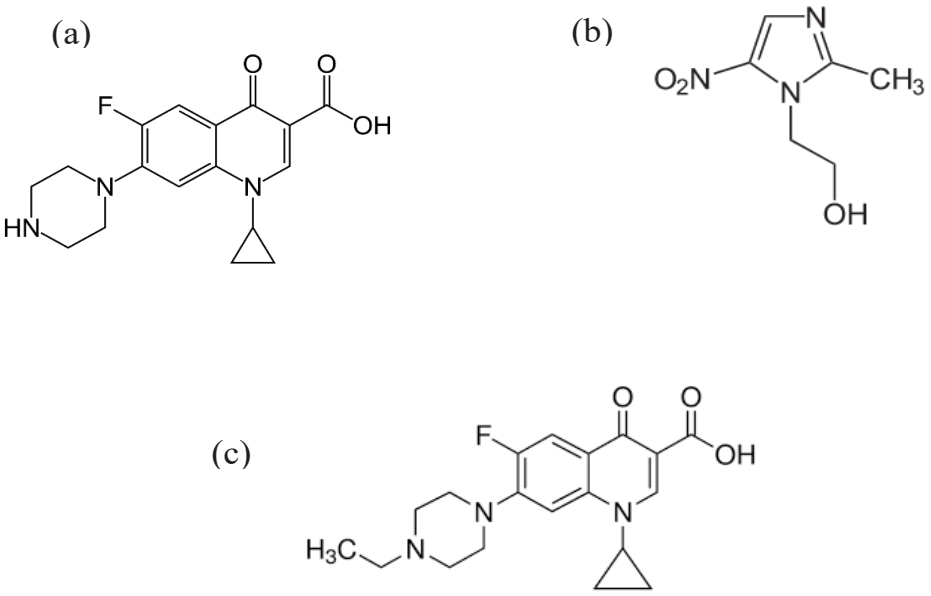


Fig. 1. The structure of a) Ciprofloxacin b) Metronidazole

resistance issues by integrating ZnO nanoparticles into our formulation. All three components were loaded in PVP-PEG to produce CFMZ-PVP-PEG@ZnO nanohybrid, which was further studied for its drug-release kinetics. In addition, environmental stimuli, including ionic strength and pH effect on drug release were evaluated. The drug-loaded PVP-PEG@ZnO nanohybrids were characterized for their particle size, morphology, drug-loading, and release mechanism. Furthermore, an investigation of the comparative effects of PEG and PVP-PEG-capped ZnO nanohybrids on release and antibacterial activities was conducted.

Additionally, a molecular-level computational approach was applied to understand the adsorption of the drug on the nanohybrid. The developed drug-loaded PVP-PEG@ZnO nanohybrid indicated significant behavior due to the presence of PVP polymer as an ionic- and pH-responsive polymer.

## MATERIALS AND METHODS

*Materials*

Poly (vinyl pyrrolidone) PVP K130 and poly (ethylene glycol) (PEG) (MW=6000,10000) were purchased from Sigma Aldrich. Zinc nitrate hexahydrate $Zn(NO_3)_2.6H_2O$, zinc acetate dihydrate Zn(COO)ammonia solution (25% Scharlau) were obtained from Merck. Daroupakhsh Pharmaceutical Company, Iran, provided enrofloxacin, ciprofloxacin, and metronidazole (purity of 99.7%). Phosphate buffered saline (PBS) (pH: 1.7, 2.5, and 6.8) was prepared using sodium phosphate monobasic, two basic crystals, and phosphoric acid.

*Preparation of CFMZ-ZnO/PVP-PEG nanohybrid*

The drug-loaded PVP-PEG@ZnO hybrid system was synthesized using a modified sol-gel and co-precipitation method following the procedure shown in Fig. 2 [19]. Briefly, (150 mL) of polymeric (0.2% w/v) solution was prepared by dissolving PEG (MW=6000) and PVP in 150 mL of deionized water. The solution was stirred, and 1 g zinc nitrate ($Zn(NO_3)_2$) was added. Both the drugs, CF and MZ, were dissolved in this solution at varying drug: polymer ratios of 0.3, 0.6, and 1. After that, 1.7 mL of ammonia solution ($NH_4OH$) was added drop-wise into the solution under vigorous and constant stirring at room temperature until colloidal particles appeared. The colloidal solution was refluxed at 70 -90 °C for 2-3h. After cooling down, the formed precipitates were centrifuged and washed with deionized water and ethanol three times to remove impurities. The final product was dried in a hot air oven at 85 °C. For comparison, drug-free PVP-PEG@ZnO hybrid systems were prepared using the same procedure. The following formulations are mentioned in the table1: (PVP/PEG)-$(CF/MZ)_{1.25}$-ZnO, (PVP/PEG)-$(CF/MZ)_{1.11}$-ZnO, (PVP/PEG)-$(CF/MZ)_2$-ZnO.

*Preparation of EFX- PEG@ ZnO hybrid system*

Spherical assemblies of ZnO nanoparticles were prepared in poly (ethylene glycol) (PEG) (MW=10000) solution incorporated with enrofloxacin (EFX) using sol-gel method. Briefly, mol of poly(ethylene glycol) (PEG) and 30 mg EFX were dispersed into 20 mL deionized water and stirred with a magnetic stirrer to obtain a clear

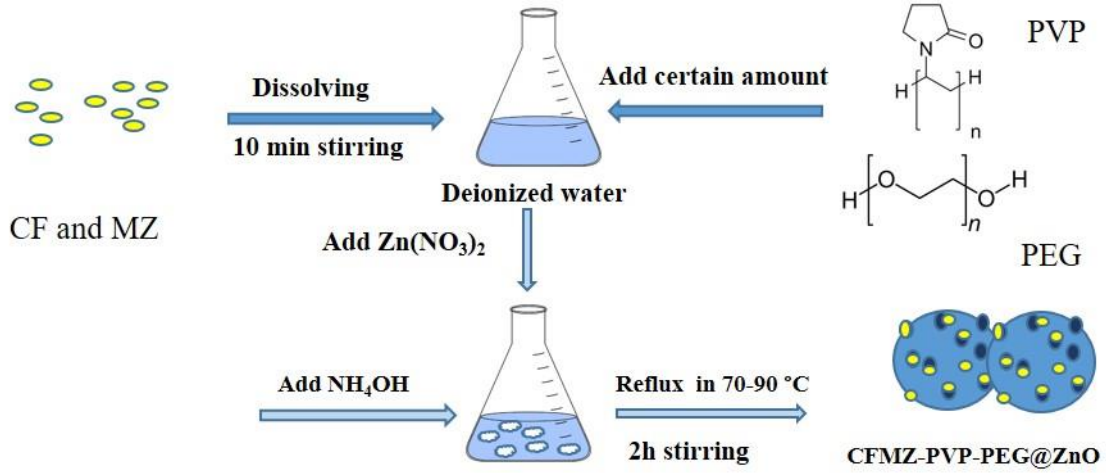


Fig. 2. The formation of CFMZ@ZnO hybrid in PVP and PEG network

homogeneous solution. 5.48 g of zinc acetate dihydrate was dissolved in 50 mL ethanol at 50 °C and mixed with the above 20 mL of EFX-PEG solution. 10 mL of 1M sodium hydroxide solution was added dropwise to the mixture under vigorous stirring at room temperature for 2h. The solid product was separated by centrifugation at 14000 rpm for 2min, washed with ethanol and distilled water several times to remove unreacted materials, and air-dried at ambient temperature for 24 h. The polymeric-zinc oxide-EFX materials were denoted as EFX-PEG@ZnO.

*Characterization techniques*

Fourier transform infrared spectroscopy (FT-IR) (Bruker, Equinox 55, Germany) was recorded between 550 and 3900 $cm^{-1}$ using a KBr wafer to investigate the chemical interactions between drugs polymers and the ZnO matrix. The spectra of drugs (CF and MZ), polymer, drug-free-loaded nanoparticles, and drug-loaded nanoparticles were recorded.

The morphology of the drug-loaded hybrids was investigated using field emission scanning electron microscopy (FESEM, MIRA3 TESCAN) at 135kx, after sputter coating the samples with gold.

The particle size analysis and size distribution were determined using dynamic laser scattering (DLS) equipment (Horiba, SZ-100, Japan). The nanohybrids were dispersed in distilled water by probe ultrasonic for 1 min before analysis. The particle size evaluation was carried out at 25 °C by He-Ne laser at 90º scattering angle.

Thermal gravimetric analysis (TGA) was carried out using a PL thermo-gravimetric analyzer (SDT Q600 V20.9 Build 20). The samples were heated from 20 to 800 °C at a heating rate of 10 °C/min under air.

*Antimicrobial activity assay*

Antibacterial efficacy of drug-free, drug-loaded PEG@ZnO, and PVP-PEG@ZnO hybrids was evaluated against two Gram-positive bacteria, Staphylococcus aureus (ATCC 25923) and Bacillus subtilis (ATCC 6633), and one Gram-negative bacteria, Escherichia coli (ATCC25922) using agar diffusion method in sterile Petri dishes [20]. Stock bacterial cultures were prepared by inoculating the strains in Tryptone Soya Agar (TSA), followed by incubation at 35 °C for 24 h. These cultures were at 4 °C until use. Working cultures were obtained by transferring a loopful from the stock culture into 5 mL of Brain Heart Infusion broth (BHI) and incubating at 35 °C for 24 h.

Subsequently, 50 µL of an aqueous working culture (at approximately CFU/mL) was added to the agar plates. The plates were kept at 37 °C incubator for 24h. The respective solvent and tetracycline ($1mg.mL^{-1}$) were served as negative and positive controls, respectively. Antimicrobial activity of the nanohybrids was evaluated by measuring their inhibition zones due to subsiding bacterial growth around each sample.

*Drug –loading content*

The efficacy of drug encapsulation was determined by shaking (60rpm) 100 mg of drug-loaded hybrid in 10 mL PBS solution (0.2M, pH=1.7) at 37 ºC for 24 h, followed by centrifugation (11,000 rpm for 2 min) and evaluation of released drugs in the diluted supernatant. The amount of CF and MZ in the supernatant (encapsulated drug) was determined using a UV-Vis spectrophotometer (Optizen 3220UV, Korea) at a maximum wavelength of 280 nm and 320 nm using the calibration curve. Drug loading (DL) content was calculated by the following equations:

$$\%DL = \frac{weight\ of\ drug\ encapsulated}{weight\ of\ nanoparticles} \times 100 \quad (1)$$

TGA instrument (New Castle, DE, USA) was also employed to calculate the drug payload efficiency.

*In vitro release experiments*

The in vitro drug release studies were conducted at the physiological temperature of 37 °C and in different pH environments (pH 1.7, pH 2.5 and pH 6.8) using batch-based methods. The buffer solution with different pH was provided using PBS and phosphoric acid. Typically, 100 mg of the drug carrier was soaked in 10 mL dissolution media: enzyme-free simulated gastric fluid (SGF, 10 mM, pH 1.7 and pH 2.5) and enzyme-free simulated intestinal fluid (SIF, 10 mM, pH 6.8) in a test tube. The test tubes were placed in an orbital shaker- incubator (Rotator 2000, Behdad) at 37 °C with a shaking speed of 65 rpm. At different time intervals, the samples were centrifuged at 11,000 rpm for 2 min. UV-Vis (Optizen 3220UV, Korea) spectrophotometer was used to determine the amounts of released CF and MZ at two separate wavelengths of 270 nm and 320 nm. The impact of ionic strength on the drug release was investigated

following the same procedure in SIF buffer solution (20 mM, pH 6.8).

*Mathematical modeling of drug release*

Seven different kinetic models, mainly non-Fickian diffusion-controlled process, two empirical exponential equations and three semi-empirical models derived from Fickian diffusion, were fitted to the drugs' release data using non-linear regressions. The Akaike's information criterion (AIC) was calculated for each model as an indicator to investigate the best model for a given dataset [21].

*Error analysis*

It is essential to use error analysis to verify the fit quality of fit of the best drug release data model. The four error functions employed in this work are residual root mean square error (RMSE), sum of the absolute error (SAE), average relative error (ARE), and average relative standard error (ARS). The smaller the error function value, the better the fit of the curve fit. The expressions of error functions are as follows [22]:

(i) Residual root mean square error (RMSE):

$$RMSE = \sqrt{\frac{1}{n-2}\sum_{i=1}^{n}(q_{exp} - q_{cal})^2} \quad (2)$$

Where n is the number of experimental data points, is the calculated data, is the experimental data.

(i) Sum of the absolute error (SAE):

$$SAE = \sum_{i=1}^{n}\left|(q_{cal} - q_{exp})\right|_i \quad (3)$$

Average relative error (ARE):

$$ARE = \frac{1}{n}\sum_{i=1}^{n}\left|\frac{q_{cal} - q_{exp}}{q_{exp}}\right| \quad (4)$$

(ii) Average relative standard error (ARS):

$$ARS = 100 \times \sqrt{\frac{\sum_{i=1}^{n}((q_{cal} - q_{exp})/q_{exp})^2}{n-1}} \quad (5)$$

*Computational details*

In order to study interactions between drugs with polymers and matrix, the electronic structures of molecules and the prepared nanoparticles were investigated by density functional theory (DFT) at B3LYP/LanL2DZ level of theory. Gaussian 09 program package was applied to optimize the complexes [23].

*Molecular dynamic simulations*

Molecular dynamic (MD) simulations were used to compare the interactions of CF and MZ drugs with the PVP-PEG@ ZnO hybrid. These interactions were also studied in an aqueous phase, where the release of the drugs was compared in water. MD simulations were carried out using the Forcite module of Materials Studio. The bonded and non-bonded interactions were modeled based on the DREIDING force field [24]. This force field has been widely used to describe the structures and dynamics of organic and biological molecules. The size of the simulation box was set at 31.70 Å × 31.70 Å × 31.70 Å, and periodic boundary conditions were applied to avoid any arbitrary boundary effects. Simulations were performed in the NVT (constant number of particles, consistent volume, and constant temperature) ensemble with a time step of 1 fs and 3500 ps simulation time.

First, the ZnO nanoparticles with a diameter of 14 Å along with the proper amount of the drug molecules, PVP and PEG (based on their molar ratios in the experimental section), were placed in the unit cell. Before MD simulation calculations, the configuration of the unit cell was optimized using the Smart algorithm. After the equilibration process, the interaction energy of the drugs and PVP-PEG@ZnO in the resulted solid hybrid (drug-loaded PVP-PEG@ZnO hybrid) was evaluated according to the following equation:

$$E_{int} = E_{Hybrid+Drug} - \left(E_{Hybrid} + E_{Drug}\right) \quad (6)$$

Where , and are the obtained average energies from the MD simulations of the drug-loaded PVP-PEG@ZnO hybrid, drug-free PVP-PEG@ZnO hybrid, and the drugs, respectively.

In the next step, the interaction of the drug-loaded PVP-PEG@ZnO hybrid (obtained in the previous step) with water molecules was studied. For this purpose, the $H_2O$ molecules were added to the unit cell (about 700 $H_2O$ molecules) so that water molecules completely surrounded the drug-loaded PVP-PEG@ZnO hybrid.

The interaction energy of drugs with PVP-PEG@ ZnO hybrid in aqueous solution was obtained

according to the following equation:

$$E_{int,aq} = E_{Hybrid+Drug+H2O} - (E_{hybrid+H_2O} + E_{Drug}) \quad (7)$$

Where and are the obtained average energies from the MD simulations of the drug-loaded PVP-PEG@ZnO hybrid and drug-free PVP-PEG@ZnO hybrid in the aqueous solution, respectively.

## RESULTS AND DISCUSSION

### *Physico-chemical characterization of the prepared PVP-PEG@ZnO hybrids*

Fig. 2 shows the synthesis procedure of polymeric drug-loaded PVP-PEG@ZnO hybrid designed for a broad-spectrum antimicrobial activity that possesses not only fluoroquinolone, but also metronidazole, in order to study its effectiveness against both Gram-negative and Gram-positive bacteria. Moreover, studies have indicated the excellent antimicrobial potential of ZnO nanoparticles when used in combination with beta-lactams and amino glycosides against different pathogenic microbes [20]. Therefore, here we combined ZnO with antibiotics to offer synergistic activity of drugs and nanoparticles and pave the way for suitable design of drug carriers. The deprotonation/protonation switchability of PVP devotes the nanohybrids with good pH- and ionic strength- dual sensitivity in the drug delivery.

### *FT-IR spectroscopy analysis*

The FT-IR spectroscopy was applied to affirm the intermolecular bonds of drugs into ZnO nanoparticles (Fig. 3). FTIR spectra of pure PVP-PEG@ZnO system (shown with (a)) illustrates an IR peak at 547 $cm^{-1}$ due to the stretching vibration of ZnO conjugation with polymer. The appearance of a broad absorption band at 3377 $cm^{-1}$ is due to absorption of -OH group in ZnO and PEG in drug-free and drug-loaded CFMZ-PVP-PEG@ZnO composite, which indicates binding of PEG with ZnO and intermolecular bonds through encapsulation process [25]. The characteristic bands at 1367 $cm^{-1}$ and 1271 $cm^{-1}$ in the FTIR spectrum of 2c and 2d are due to N-O stretching vibration and C-F group

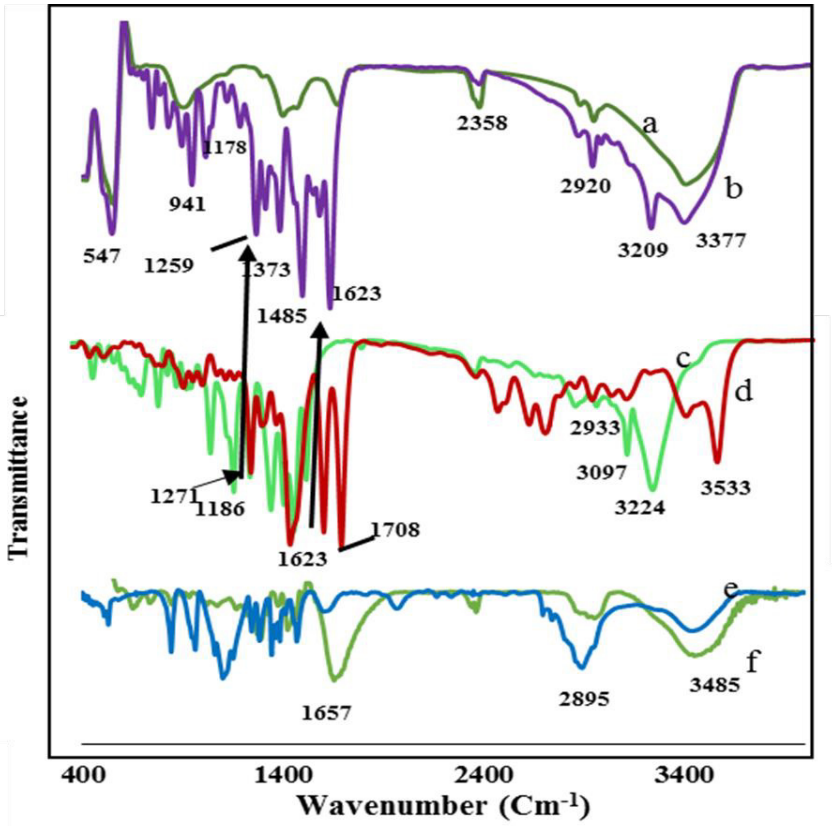


Fig. 3. FT-IR spectra of a) pure ZnO/PEG-PVP, b) drug loaded- ZnO/PEG-PVP, c) Metronidazole, d) Ciprofloxacin, e) PEG, f)PVP

stretching that appeared at 1373 $cm^{-1}$and 1259 $cm^{-1}$ in FTIR spectrum of drug-loaded PVP-PEG@ ZnO composite (spectrum b). It might be due to the interaction of the electron-doner fluorine atom in ciprofloxacin with the Zn atom. The bands at 1708 $cm^{-1}$ and 1623 $cm^{-1}$ in the spectrum of CF were attributed to the carbonyl C=O stretching and the quinolones. Instead, the strong peak at 1623 $cm^{-1}$ emerged, and the band at 1708 $cm^{-1}$ vanished due to the interaction between CF and ZnO in drug-loaded nanohybrids. A peak at 1186 $cm^{-1}$ (due to C-O stretching) was shifted to 1178 $cm^{-1}$, and its intensity was decreased. The bands at 2933 $cm^{-1}$ in the spectrum of CF, 2933 $cm^{-1}$, 3097 $cm^{-1}$ assigned to stretching =CH and 3224 $cm^{-1}$ to stretching –OH in the spectrum of MZ, were changed to 2920 $cm^{-1}$ and 3209 $cm^{-1}$ (corresponding to H-bonding) in drug-loaded PVP-PEG@ZnO nanoparticles. These observed changes in the IR spectrum of drug-loaded PVP-PEG@ZnO nanohybrid confirm the successful co-encapsulation of CF and MZ in ZnO hybrid system. As reported in the literature [26-28], CF has two metal binding sites coordinated through two carbonyl oxygen atoms in all the complexes. As well, MZ has four sites for metal bonding.

*Field emission scanning electron microscopy (FE-SEM)*

FE-SEM images of the CFMZ-PVP-PEG@ZnO and EFX-PEG@ZnO hybrid system are shown in Fig. 4a-d. These images were captured to investigate morphological changes in the shape and size of the composites. The CFMZ-PVP-PEG@ZnO composite prepared by the prob sonicator showed hexagonal structures with an average size of about 300 nm (Fig. 4b). This size was in agreement with the obtained size determined via dynamic light scattering (DLS, 180-321 nm). It could be seen from the SEM images that the heterogeneity surface of composite in Fig. 4a had transformed to uniform particles with homogeneous surfaces. Fig. 4a and 4c present typical FE-SEM images of CFMZ-PVP-PEG@ZnO composites prepared by a magnetic stirrer with different surface morphology and heterogeneity surfaces. Fig. 4a exhibits a smooth and layered lamellar surface of hybrids at low magnification. At higher magnification (Fig. 3c), the hybrid particles show agglomerates with connected cylindrical particles and small structured

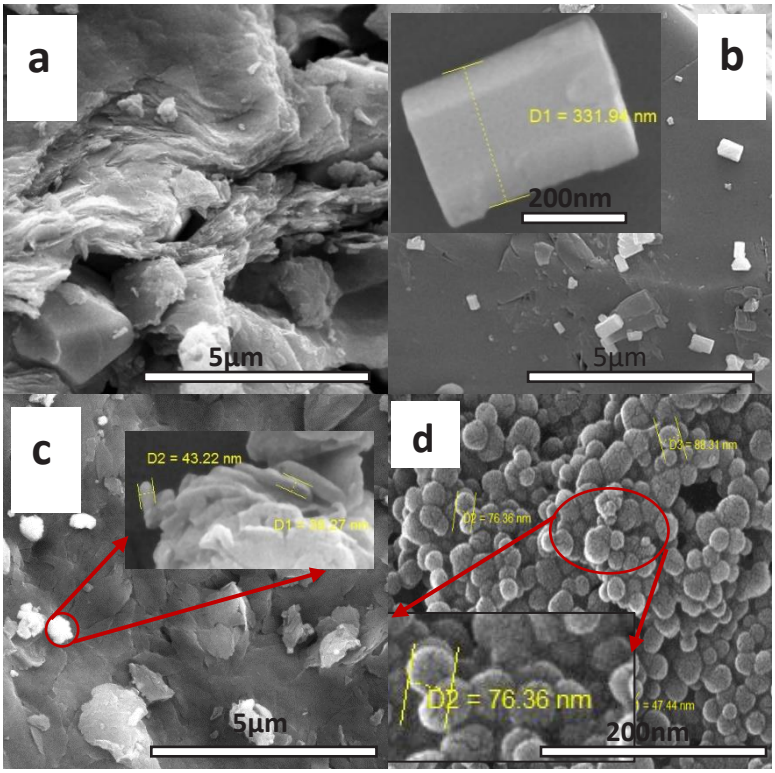


Fig. 4. FE-SEM images of the drug-loaded CFMZ-PVP-PEG@ZnO hybrids a) sample1, (b) sample 2 prepared under prob sonicator, (c) sample 3 and (d) EFX- PEG@ZnO

Table 1. Characterization and antibacterial activity of zinc oxide hybrids

| | Zone of inhibition (mm) against bacterial strains | | | | | |
|---|---|---|---|---|---|---|
| Sample | S. Aureus | B. Subtilis | E. Coli | Drug/Polymer | LC (%) (CF) | LC (%) (MZ) |
| PVP-PEG@ZnO | 30 | 45 | 43 | - | - | - |
| 1 | 23 | 40 | 40 | 0.3 | 28.07 | 24.18 |
| 2 | 31 | 45 | 45 | 0.6 | 31.69 | 24.39 |
| 3 | 32 | 46 | 50 | 1 | 22.23 | 30.97 |
| Tetracyclin (Standard) | 38 | 30 | 37 | - | - | - |
| PEG@ZnO | 22 | - | 20 | 0.3 | 14 | - |

particles of irregular morphology. However, there is a dense aggregate of primary ZnO nanoparticles. The incorporation of PVP into the hybrid network resulted in the formation of larger-sized particles. Fig. 4d shows FE-SEM images of EFX-PEG@ZnO composite. This figure shows that drug-loaded PEG@ZnO nanoparticles were spherical in shape, with a diameter of ~36-76 nm. Clear and uniform morphology was observed for the drug-loaded ZnO nanoparticles in the presence of PEG.

*Thermogravimetric analysis (TGA)*

TGA, differential thermal analysis (DTA), and UV spectrometry were applied to quantify actual drug loading. The TGA and DTA curves of drugs, drug-free hybrid system (PVP-PEG@ZnO), and drug-loaded hybrid system (CF-MZ-PVP-PEG@ZnO) are illustrated in Fig. 5a and 5b. The drug loading amount using two techniques is presented in Table 1.

The percentage of drug entrapment was determined from the mass loss with respect to the total initial mass between 20 and 800 ºC. The DTA curve of MZ shows two endothermic and exothermic peaks from 163 ºC to 280.78 ºC. In TGA curve of MZ, the mass loss percentage from 159 ºC to 271 ºC is due to the elimination of $NO_2$ and $C_2H_5OH$ groups. The decomposition from 272 ºC to 306 ºC is assigned to the loss of $C_3H_3N_2$ [29]. In DTA curve of CF, one endothermic peak at 157

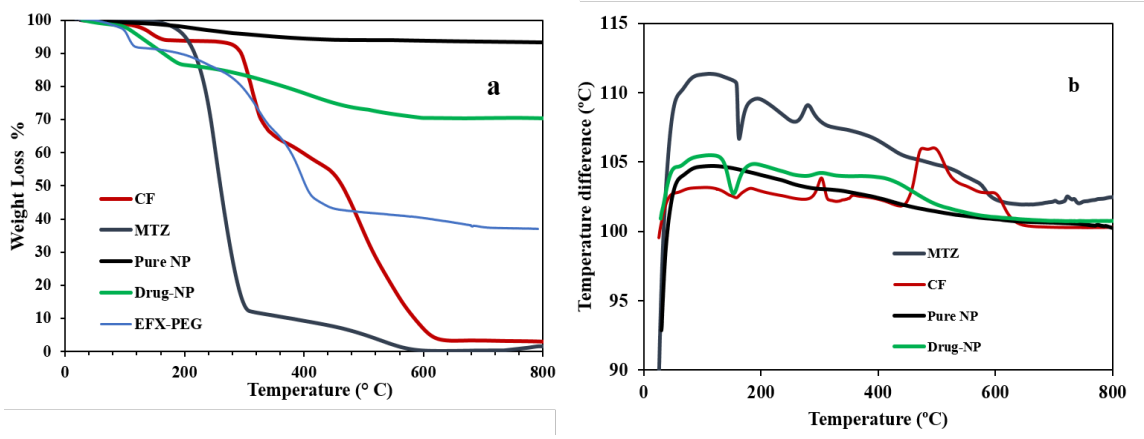


Fig. 5. TGA (a), DTA (b) curves of CFMZ-PVP-PEG@ZnO and (c) EFX- PEG@ZnO

ºC is due to the removal of $C_2H_2$ group. The two peaks at 302 and 361 ºC are related to the mass loss of drug residuals [30].

The decomposition of pure PVP-PEG@ZnO and drug-loaded CFMZ-PVP-PEG@ZnO hybrid system starts at 30 ºC. The decrease in the curve from 30 ºC to 100 ºC may be due to the evaporation of absorbed water by the hybrid system. The mass loss difference between pure PVP-PEG@ZnO and drug-loaded CFMZ-PVP-PEG@ZnO nanohybrids in TGA curves resulting from drug loading was approximately 22.95%. In TGA and DTA curves of drug-loaded CFMZ-PVP-PEG@ZnO, the decline in the curve at the temperature range of 136 to 203 ºC may be primarily attributed to the loss of MZ that is accompanied by weight loss of 11%. The weight loss between 200 and 250 ºC, is related to the removal of the residual ethoxy groups (-OEt) and MZ residue [29]. The one endothermic peak at 304 ºC and the decomposition event on the related TGA curves in the temperature range of 257 ºC to 422 ºC may be due to the mass loss of CF which is almost equal to 10.25%.

*In vitro antibacterial activity evaluation of PVP-PEG@ZnO hybrids*

The antibacterial activity of all the four types of PVP-PEG@ZnO hybrids and EFX-PEG@ZnO nanoparticles is shown in Table 1 in terms of the inhibition zone (mm) of the synthesized PVP-PEG@ZnO hybrids and EFX-PEG@ZnO nanoparticles. The images of the antibacterial performance of hybrids after 24 h of incubation are displayed in Fig. 6. According to the results, it is clear that all of the hybrid formulations have antimicrobial activity. More activity was demonstrated by hybrids against Gram-positive bacteria (Bacillus subtilis) and Gram-negative bacteria (Escherichia coli) with an inhibition zone of 46 mm and 50 mm, respectively. Drug-free PVP-PEG@ZnO hybrid showed more growth inhibition than from that of tetracyclin control. This confirms the potential of PVP-PEG@ZnO composite to kill bacteria. However, by increasing the amount of antibiotics in drug-loaded CFMZ-PVP-PEG@ZnO hybrids, the inhibition zone has been further enhanced. As shown in Fig. 6, the growth inhibition ranged between 30 and 50 mm

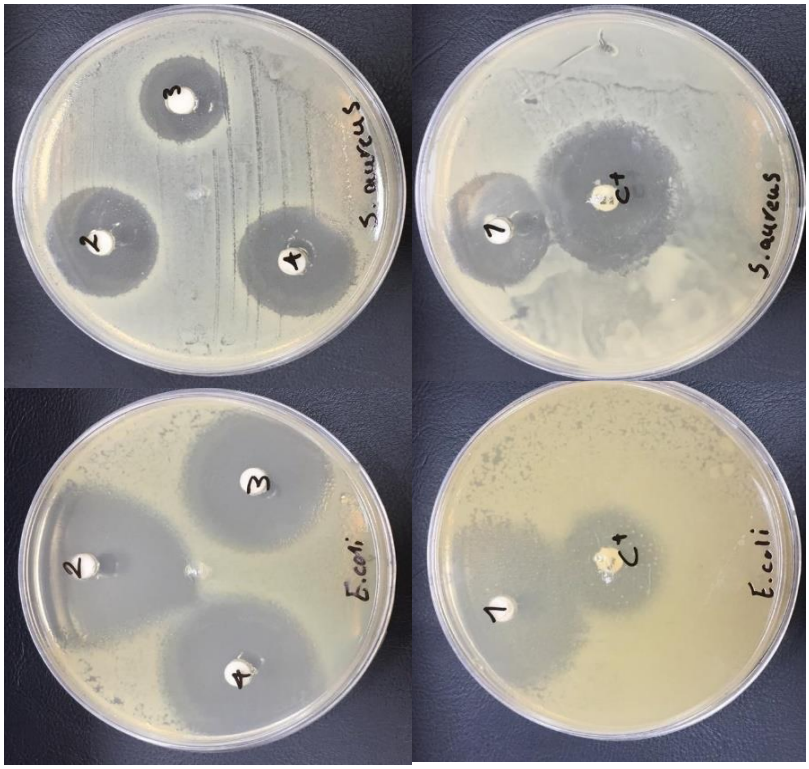


Fig. 6. Antimicrobial activity of drug-loaded CFMZ-PVP-PEG@ZnO hybrids: 1) drug/polymer: 1, 2) drug/polymer:0.6, 3) drug/polymer:0.3, 4) drug-free PVP-PEG@ZnO hybrid against three bacterial strains

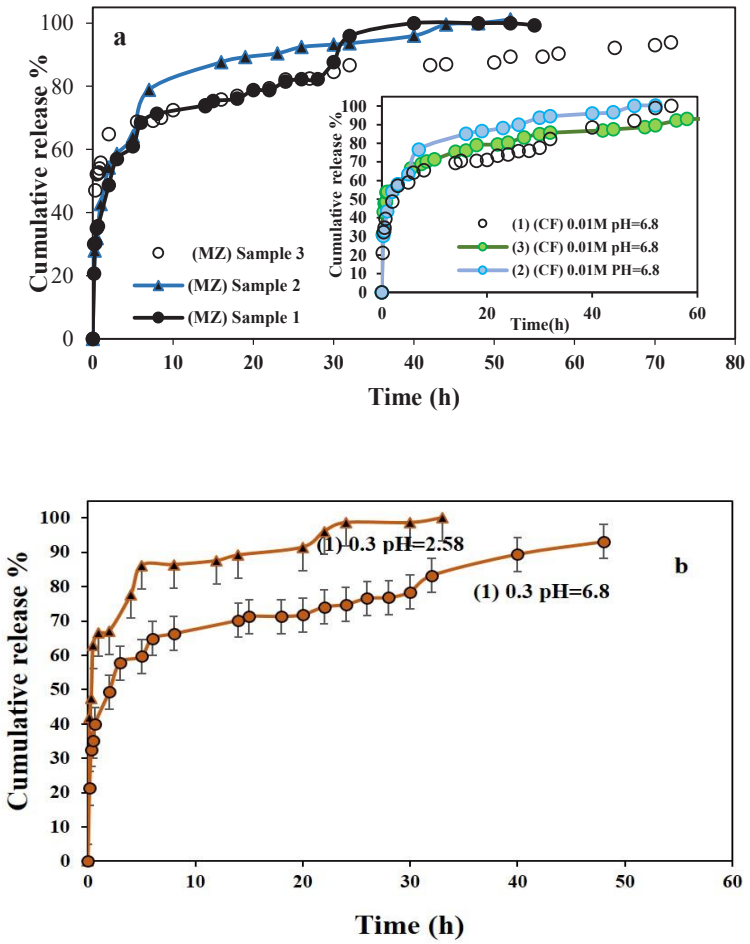


Fig. 7. (a) The release profiles of CF and MZ from all three samples (pH=6.8) and (b) The release profile of CF from sample 1 in two pH.

with the hybrid concentration of 50 µg/mL, as the minimum inhibitory concentration (MIC). These results reveal a good activity and better growth inhibitory effect of PVP-PEG@ZnO as compared to EFX-PEG@ZnO nanohybrids and those reported in other studies for capped ZnO nanoparticles with surfactants having 10-26 mm of antibacterial activity [24, 36].

*In vitro drug release studies*

The in vitro study was performed at 37 ± 0.5 °C in the buffer solution (pH 1.7, 2.58, and 6.8). Fig. 7a displays the release patterns of CF and MZ from the different drug-loaded CFMZ- PVP-PEG@ ZnO hybrids in (10 mM, pH=6.8) buffer solution as a function of time. An initial burst release was observed, followed by a slow sustained release. The initial release of CF and MZ from hybrids with drug/polymer ratios of 0.3, 0.6, and 1 was approximately 48%, 53%, and 53% after 2 h, respectively. Sample1 with the drug/polymer ratio of 0.3 showed a lower and distinct release pattern. The release of CF from sample1, was 64% and 69% at the sampling time of 6h and 14h, which was slower than the MZ release (68% and 74%), simultaneously. Such a burst release of the drug can be attributed to the surface adsorption of the drug in which a weak interaction would lead to the faster release. As shown in Fig. 7b, the release of CF and MZ from sample1 was very fast in pH=2.58. It reached 41% and 36% after 10 min, and 67% and 63%, within 2h. To study the effect of pH on drug release profile, we tested SIF buffer solution (pH=1.7) (Fig. 8a). pH-responsive behavior with an increase in the drug release rate by decreasing the pH of the dissolution medium. The elevated drug release at low pH can be attributed to the higher swelling ratio of PVP at a low pH value. Calibration

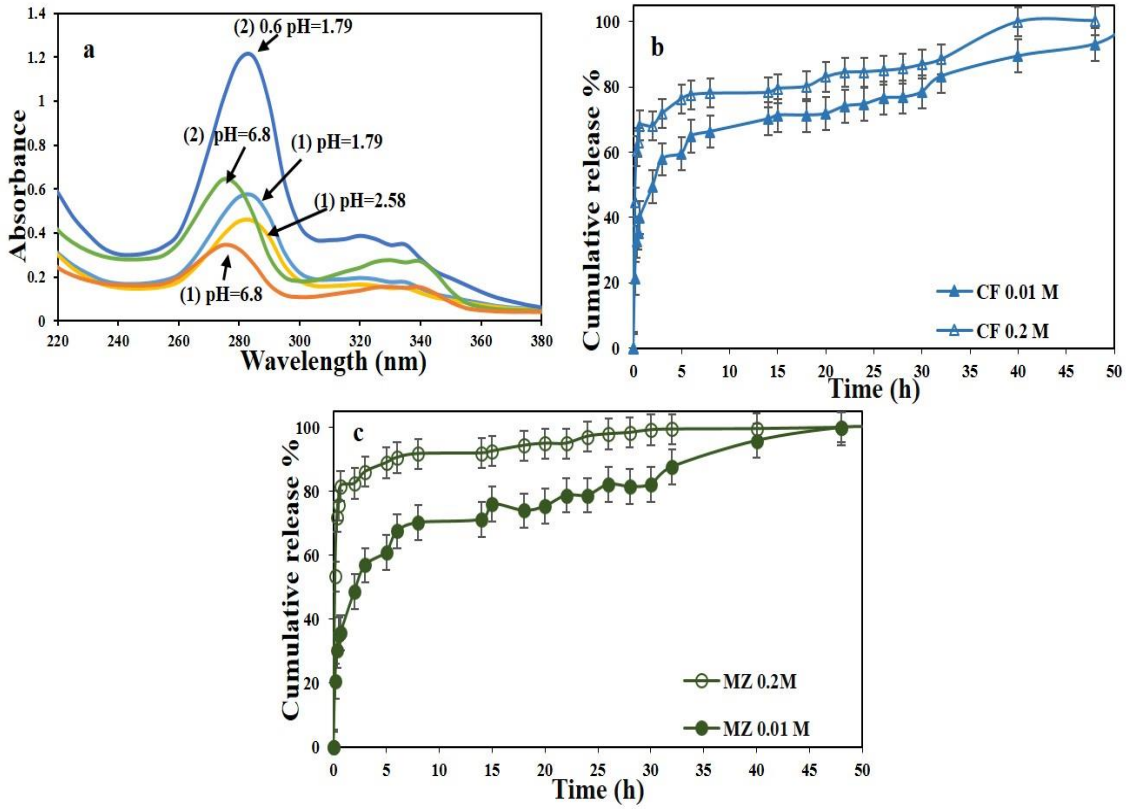


Fig. 8. (a) Effect of pH on drug release in two formulations and (b) The impact of ionic strength on drug release rate

curves of drugs are presented in supporting information, Fig. S2.

Ionic strength, pH, and particle surface chemistry are major parameters that significantly affect drug release behavior and mobility of nanoparticles [31, 32]. In order to evaluate the impact of dissolution medium ionic strength, the release studies were conducted in SGF buffer solution (0.2 M, pH=6.8). The ionic strength-sensitive characteristic of nanoparticles is depicted in Fig. 8b and 7c. It is evident that with an increase in the ionic strength of the dissolution medium, the cumulative release percentage was gradually enhanced. As reported in the literature the medium ionic strength can affect hybrids using multiple mechanisms by which carriers decrease their excess surface energy. To achieve this goal, nanoparticles may cluster into dense aggregates or dissolve according to the DLVO theory and Noyes-Whitney relationships [32].

*Drug release kinetics*

The main objective of this work was to study the release kinetics and transport mechanisms of the drug release from drug-loaded CFMZ-PVP-PEG@ZnO hybrid system. Three different models including Higuchi square root plot, Ritger-Peppas, and Peppas-Sahlin equations, were used to fit the experimental data [33-35]. In order to study the quality of fit and kinetics of release, the correlation coefficient ($R^2$), AIC values, error analysis and other parameters of equations were calculated by linear and non-linear least-squares regression (Tables 2 and 3) and (supporting information, Table S1). According to the correlation coefficients, the smaller AIC values, and error analysis functions, the best fit was observed with Peppas-Sahlin equation. The graphical representation of these kinetic models for three release systems with drug/polymer ratios of 0.3, 0.6, and 1 are illustrated in Fig. 9 and (supporting information, Fig. S3). All of the kinetic models are valid, only for the first 60% of drug release. Therefore, for all three samples, the drug release was considered up to 60%. Table 2 presents the diffusional exponent (n) and the release constant (k) for MZ and CF release from

Table 2. The release parameter values obtained by fitting the in vitro release data to Peppas- Sahlin ($M_t/M_\infty = K_1t^m+K_2t^{2m}$ ) model.

| Release system | $K_1$ | $K_2$ | m | $R^2$ | AIC | RMSE | SAE | ARE | ARS |
|---|---|---|---|---|---|---|---|---|---|
| Drug/Polymer: 0.3 | | | | | | | | | |
| Ciprofloxacin | 53.18 | -10.86 | 0.38 | 0.9735 | 36.83 | 2.26 | 14.41 | 0.05 | 6.88 |
| Metronidazole | 48.51 | -7.58 | 0.38 | 0.9833 | 35.87 | 2.15 | 13.62 | 0.04 | 5.59 |
| Drug/Polymer: 0.6 | | | | | | | | | |
| Ciprofloxacin | 54.57 | -10.82 | 0.38 | 0.9958 | 23.31 | 1.54 | 6.39 | 0.03 | 8.32 |
| Metronidazole | 54.48 | -11.32 | 0.45 | 0.9970 | 21.18 | 1.32 | 5.63 | 0.02 | 4.25 |
| Drug/Polymer: 1 | | | | | | | | | |
| Ciprofloxacin | 72.83 | -20.27 | 0.32 | 0.9930 | 47.11 | 2.95 | 19.78 | 0.04 | 6.33 |
| Metronidazole | 81.35 | -23.69 | 0.4 | 0.9834 | 47.48 | 2.81 | 19.00 | 0.05 | 16.48 |

Table 3.The release parameter values obtained by fitting the in vitro release data to Ritger-Peppas ($M_t/M_\infty = Kt^n$ ) model.

| Release system | $K_1$ | n | $R^2$ | AIC | RMSE | SAE | ARE | ARS |
|---|---|---|---|---|---|---|---|---|
| Drug/Polymer:0.3 | | | | | | | | |
| Ciprofloxacin | 40.87 | 0.26 | 0.9733 | 39.23 | 2.68 | 16.50 | 0.06 | 9.39 |
| Metronidazole | 40.11 | 0.29 | 0.9824 | 34.75 | 2.22 | 14.88 | 0.04 | 6.7 |
| Drug/Polymer:0.6 | | | | | | | | |
| Ciprofloxacin | 42.88 | 0.26 | 0.9932 | 24.63 | 2.18 | 9.20 | 0.03 | 4.72 |
| Metronidazole | 41.98 | 0.29 | 0.9922 | 25.99 | 2.41 | 9.78 | 0.03 | 4.67 |
| Drug/Polymer:1 | | | | | | | | |
| Ciprofloxacin | 50.97 | 0.17 | 0.9917 | 48.89 | 3.56 | 22.21 | 0.05 | 8.83 |
| Metronidazole | 54.53 | 0.17 | 0.9850 | 54.61 | 5.20 | 35.83 | 0.08 | 12.69 |

hybrids. All the samples shown values around 0.2-0.3. As reported in the literature, in Ritger and Peppas equation, when n=0.43, the drug release is managed by Fickian diffusion, and when 0.43< n < 0.85 it is anomalous (non-Fickian) transport. These values are correct for the monodispersed polymer composites, but here polydispersed hybrids have been prepared. In polydisperse samples, Fickian diffusion mechanism can be recognized by n values < 0.43. This fact could explain, the drug release mechanism was governed by both non-Fickian diffusion and case II relaxations. As well as, non-Fickian diffusion overcame the drug release mechanism from nanoparticles. It was found that this is a two-stage process in which the Fickian contribution decreased over time. The results indicated that MZ release kinetics from hybrids is different from CF. The release mechanism of MZ is more controlled by Fickian diffusion than polymer relaxation.

*Computational analysis*

In this section, the interactions between the MZ and CF with PEG and PVP in a drug-loaded CFMZ- PVP-PEG@ZnO system as a basic model are investigated. The density functional theory (DFT) with B3LYP level and lanl2dz as a basis set was applied to all of the electronic structure calculations. To calculate BSSE value, counterpoise (CP) and non-counterpoise corrected geometry

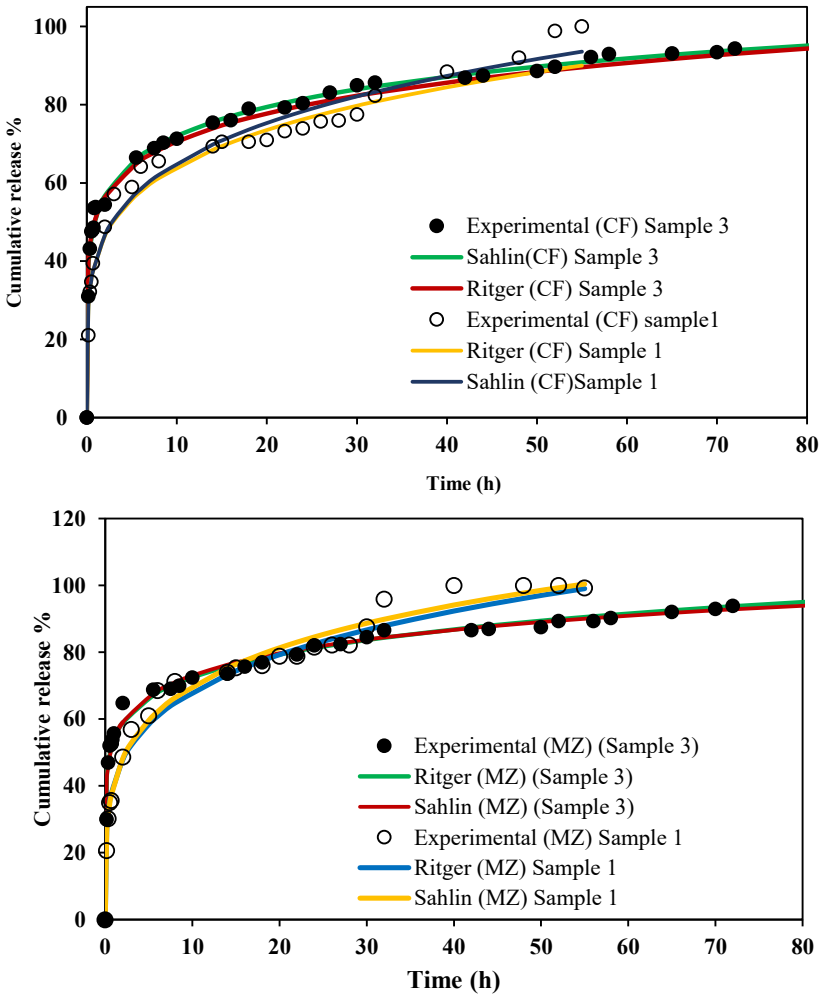


Fig. 9. The curves of drug release kinetics from samples 2 and 3 of drug-loaded ZnO/PEG-PVP hybrids.

optimizations were conducted. The energy minima on the potential energy surface were confirmed by performing the vibrational frequency analysis for all the optimized stationary points without imaginary frequency. The optimized structures of PVP-CF, PEG-CF, PEG-MZ, and PVP-MZ are shown in supporting information, Fig. S4. According to the calculated complexation energy of PVP-MZ (-17.51 kcal.mole$^{-1}$), PEG-MZ (-16.60 kcal.mole$^{-1}$), PVP-CF (-17.61 kcal.mole$^{-1}$) and PEG-CF (-15.53 kcal.mole$^{-1}$), it is observed that the intramolecular interaction between CF and PVP is stronger than MZ with PVP. As well as the PEG-MZ molecule is more stable than PEG-CF. In addition, as is shown in Fig. S4, the corresponding bond lengths (H…O) values of all the complexes, 1.59, 1.73, 1.71, and 1.75, confirm the formation of the hydrogen bond. Meanwhile, hydrophobic effects have the main role in the binding strength in supramolecular complexes. These results are due to the presence of several functional groups, such as fluorine and carboxyl groups, that are associated with high electronegative atoms. The computational results were in accordance with some drug loading capacity and encapsulation efficiency studies.

*MD simulations*

MD simulation was employed to modeled drug interaction with the PVP-PEG@ZnO hybrid system. In the first stage, after the energy minimization of the unit cell containing ZnO nanoparticles, PVP, PEG, and drug molecules, the annealing process was carried out. It was done by several simulations, in NVT ensemble, and in 1200 ps, so that initially

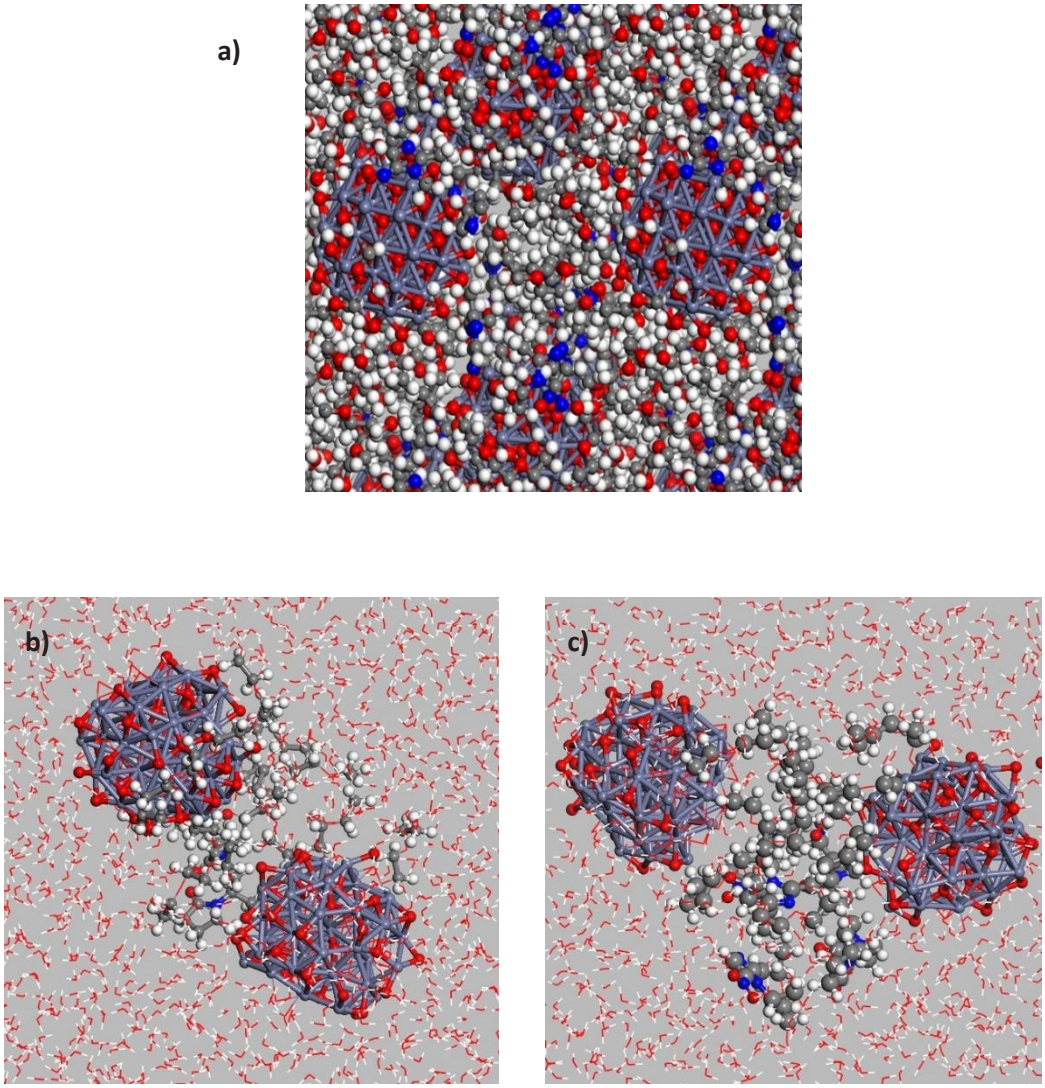


Fig. 10. (a) Solid drug-loaded hybrid and the aqueous solution of (b) CF- and (c) MZ-loaded ZnO/PEG-PVP hybrid

the temperature increased gradually from 100 K to 700 K, and then decreased gradually from 700 K to 298 K. The last simulation was done in 298 K for 3500 ps. The drug-loaded CFMZ-PVP-PEG@ZnO hybrid structure resulted from this simulation is shown in Fig. 10a. This Figure clearly indicates that PVP and PEG polymers trap the ZnO nanoparticles and prevent the nanoparticles from sticking to each other. After equilibration, the molecules, as expected, showed only vibrational motions. The calculated interaction energies between MZ and CF with ZnO/PVP-PEG hybrid were -11.13 and -16.28 Kcal.mol$^{-1}$, respectively, as evaluated by equation (7). These values show that the loaded drug in this matrix has proper interaction with polymers as well as ZnO nanoparticles. Also, the more interaction energy of CF molecules with PVP-PEG@ZnO hybrid justifies that more of this drug is trapped in the hybrid.

In the next step, the drug-loaded hybrid was placed in water to investigate the interactions in an aqueous solution (Fig. 10b and 10c). Furthermore, this simulation helps to compare the release of drug molecules in water. The interaction energy of the drug molecules with PVP-PEG@ZnO hybrid and $H_2O$ molecules was -38.24 and -269.45 Kcal.mol$^{-1}$, respectively, as obtained using equation (8). These results show that the interaction between functional groups of CF with hybrid is significantly increased in the aqueous phase.

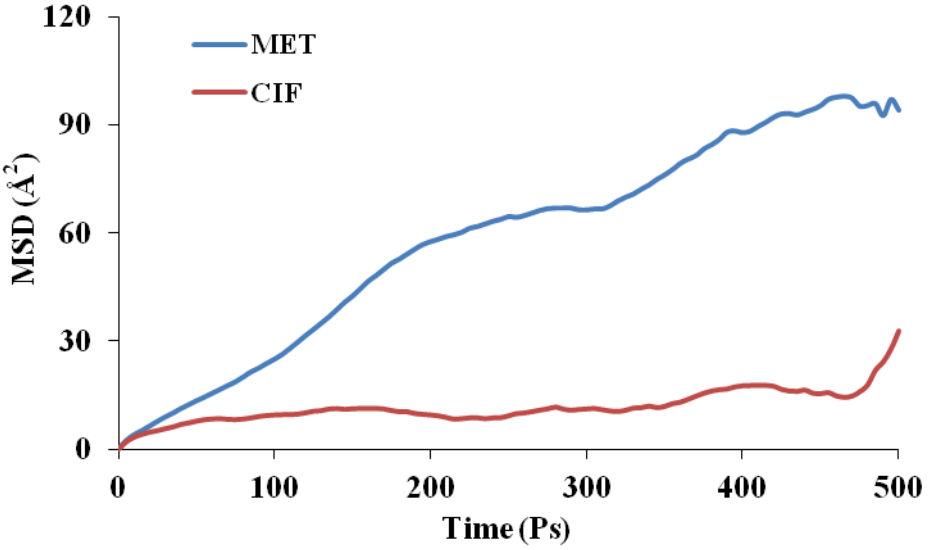


Fig. 11. Mean square displacement of drugs in the aqueous phase.

The mean square displacement (MSD) analysis was done for embedded drugs when the solid hybrid was placed in the water. The MSD is a measure of the movement of molecules relative to a reference position over time. Fig 11, shows the MSD plot vs time for two drugs. The displacement of drug molecules eventually results in the release of them in the solution. A comparison of the two drugs' displacement in this plot shows that MZ molecules had more movement during this time. The surveying of the molecules' trajectory in the simulation also clearly shows more movement and faster release of MZ molecules. This is entirely consistent with our experimental results and could be due to the smaller size of the MZ molecules and their weaker interaction with PVP-PEG@ZnO hybrid.

## CONCLUSION

In this study, non-toxic, biodegradable, multifunctional nanohybrids were successfully fabricated by self-assembly of a pH-sensitive PVP and PEG onto ZnO nanoparticles for encapsulation and controlled release of two model antibiotics in the absence of any organic solvent. Three different ratios of drug-loaded ZnO hybrid conjugates were prepared by a facile sol-gel-precipitation procedure with 22%-31% drug entrapment efficiency. The drug-loaded ZnO hybrid showed broad-spectrum antimicrobial activity against Gram-negative E. coli and Gram-positive B. Subtilis, during which sample 3 of drug-loaded ZnO hybrids with higher drug concentration indicated the best antibacterial activity. The release of drugs from intelligent hybrid system indicated pH - and ionic-strength-sensitive behavior. MZ and CF release from hybrids was increased by lowering the pH from 6.8 to 2.6 and 1.2 at 37 °C. When the ionic strength concentration was increased to 0.2M, the release of MZ and CF increased to 95% and 75%, respectively after 5h. In addition, the interaction of these hybrids with drugs was modeled by molecular dynamics simulations in solid and water environments. The experimental data and the MD simulation results are in complete agreement with each other. These data indicate that the interaction between polymers and CF is stronger than that with MZ.

## ACKNOWLEDGEMENTS

The authors gratefully acknowledge Iran National Science Foundation (INSF) and Yazd University for their financial support.

## CONFLICT OF INTEREST

The authors declare that there is no conflict of interests regarding the publication of this manuscript.

## REFERENCES

1. Espanol L, Larrea A, Andreu V, Mendoza G, Arruebo M, V. Sebastian et al., Dual encapsulation of hydrophobic and hydrophilic drugs in PLGA nanoparticles by a single-step method: drug delivery and cytotoxicity assays. RSC Adv, 2016;

6(112):111060-111069.
2. He Y, Shao L, Hu Y, Zhao F, Tan S, He D, Pan A, Redox and pH dual-responsive biodegradable mesoporous silica nanoparticle as a potential drug carrier for synergistic cancer therapy. Ceram Int., 2020, 47:4572-4578.
3. Ebadi A, Rafati AA, Bavafa S, Mohammadi M, Kinetic and theoretical studies of novel biodegradable thermo-sensitive xerogels based on PEG/PVP/silica for sustained release of enrofloxacin. Appl Surf Sci, 2017, 425:282-290.
4. Rafati AA, Ebadi A, Bavafa S, Nowroozi A, Kinetic study, structural analysis and computational investigation of novel xerogel based on drug-PEG/$SiO_2$ for controlled release of enrofloxacin. J Mol Liq, 2018, 266:733-742.
5. Hariharan R, Senthilkumar S, Suganthi A, Rajarajan M, Synthesis and characterization of doxorubicin modified ZnO/PEG nanomaterials and its photodynamic action. J Photochem Photobiol B 2012, 116:56-65.
6. Rungby J, Zinc, zinc transporters and diabetes, Diabetologia 2010, 53:1549-1551.
7. Azarudeen RS, Thirumarimurugan M, Athmiya KP, Monisha R, Prashanthini V, Antibacterial chitosan–copolymer membranes for drug delivery: Synthesis, characterization, drug release profile and its kinetics. J Chem Technol Biotechnol, 2016, 92:1659-1666.
8. Rezk AI, Obiweluozor FO, Choukrani G, Park CH, Kim CS, Drug release and kinetic models of anticancer drug (BTZ) from a pH-responsive alginate polydopamine hydrogel: Towards cancer chemotherapy. Int J Biol Macromol 2019, 141:388-400.
9. Jaisankar E, Pavithra ME, Krishna S, Thirumarimurugan M, Azarudeen RS, Dual property of chitosan blended copolymer membranes: Antidiabetic drug release profile and antimicrobial assay, Int J Biol Macromol, 2020, 145:42-52.
10. Fathi M, Akbari B, Taheriazam A, Antibiotics drug release controlling and osteoblast adhesion from Titania nanotubes arrays using silk fibroin coating, Mater Sci Eng C 2019, 103:109743.
11. Bielas R, Siewniak A, Skonieczna M, Adamiec M, Mielanczyk L, Neugebauer D, Choline based polymethacrylate matrix with pharmaceutical cations as co-delivery system for antibacterial and anti-inflammatory combined therapy. J Mol Liq 2019, 285:114-122.
12. Kumar D, Saikia AK, Kaur B, Mandal UK, Tuneable thermoresponsive hybrid magnetic nanoparticles: preparation, characterization and drug release characteristics, J. Chem. Technol. Biotechnol. 2016, 92:1006-1016.
13. Pacheco H, Vedantham K, Young A, Marriott I, Ghannam A, Tissue engineering scaffold for sequential release of vancomycin and rhBMP2 to treat bone infections, J. Biomed Mater Res – Part A 2014, 102:4213-4223.
14. Pettinelli N, Rodriguez- Liamazares S, Farrag Y, Bouza R, Barral L, Feijoo-Bandin S, Lago F, Poly(hydroxybutyrate-co-hydroxyvalerate) microparticles embedded in κ-carrageenan/locust bean gum hydrogel as a dual drug delivery carrier, Int J Biol Macromol, 2020, 146:110-118.
15. Khuroo T, Verma D, Khuroo A, Ali A, Lqbal Z, Simultaneous delivery of paclitaxel and erlotinib from dual drug loaded PLGA nanoparticles: Formulation development, thorough optimization and in vitro release. J Mol Liq 2018, 257:52-68.
16. Lebedeva IV, Washington I, Sarkar D, Clark JA, Fine RL, Dent P, Curiel DT, Turro NJ, and Fisher PB, Strategy for reversing resistance to a single anticancer agent in human prostate and pancreatic carcinomas. Proc. Nat. Acad. Sci. 2007, 104(9):3484-3489.
17. Lane D, Designer combination therapy for cancer. Nat Biotechnol, 2006, 24(2):163-164.
18. Brook I, Wexler HM, Goldstein EJ, Antianaerobic antimicrobials: spectrum and susceptibility testing. Clin Microbiol Rev, 2013, 26(3):526-54.
19. Thirugnanam T, Effect of polymers (PEG and PVP) on sol-gel synthesis of microsized zinc oxide. J nanomater, 2013, 2013:1-7.
20. Javed R, Usman M, Tabassum S, Zia M, Effect of capping agents: Structural, optical and biological properties of ZnO nanoparticles. J Appl Surf Sci, 2016, 386:319-326.
21. Yamaoka K, Nakagawa T, Uno T, Application of Akaike's information criterion (AIC) in the evaluation of linear pharmacokinetic equations. J Pharmacokinet Biopharm, 1978, 6(2):165–175.
22. Baral S, Das N, Ramulu T, Sahoo S, Das S, Chaudhury GR, Removal of Cr (VI) by thermally activated weed Salvinia cucullata in a fixed-bed column. J Hazard Mater, 2009, 161:1427–1435.
23. Frisch MJ, Schlegel HB, Scuseria GE, Robb MA, Cheeseman JR, Pople JA, et al. Gaussian 09, Revision B03, Gaussian, Inc., Wallingford CT, 2009.
24. Mayo SL, Olafson BD, Goddard WA, DREIDING: a generic force field for molecular simulations. J Phys Chem, 1990, 94 (26):8897–8909.
25. Barick K, Nigam S, Bahadur D, Nanoscale assembly of mesoporous ZnO: A potential drugcarrier. J Mater Chem, 2010, 20(31):6446-6452.
26. Obaleye J, Lawal A, Synthesis, Characterization and Antifungal Studies of Some Metronidazole Complexes. J Appl Sci Environ, 2007, 11(4):15-18.
27. Chohan ZH, Supuran CT, Scozzafava A, Metal binding and antibacterial activity of ciprofloxacin complexes. J Enzyme Inhib Med Chem, 2005, 20(3):303-307.
28. Sahoo S, Chakraborti CK, Mishra SC, Qualitative analysis of controlled release ciprofloxacin/carbopol 934 mucoadhesive suspension. J Adv Pharm Technol Res, 2011, 2(3):195-204.
29. Ali A, Elasala G, Ibrahim Synthesis R, Synthesis, Characterization, spectral, thermal analysis and Biological Activity studies of metronidazole complexes. J Mol Struct 2019, 1176:673-684.
30. Sarwade SS, Jadhav W, Khade B, Characteriztion of Novel Complex Ciprofloxacin Ag (I). Arch Appl Sci Res 2015, 7 (1):36-41.
31. Omar FM, Aziz HA, Stoll S, Aggregation and disaggregation of ZnO nanoparticles: influence of pH and adsorption of Suwannee River humic acid. J Colloid Sci Biotechnol, 2014, 468:195-201.
32. Muraleetharan V, Mantaj J, Swedrowska M, Vllasaliu D, Nanoparticle modification in biological media: implications for oral nanomedicines. RSC Adv, 2019, 9:40487-40497.
33. Higuchi T, Mechanism of sustained-action medication. Theoretical analysis of rate of release of solid drugs dispersed in solid matrices. J pharm Sci 1963, 52(12):1145-1149.
34. Ritger P, Peppas N, Simple equation for description of solute release II. Fickian and anomalous release from swellable devices. J Controlled Rrelease, 1987, 5(1):37-42.
35. Peppas NA, Sahlin JJ, A simple equation for the description of solute release. III. Coupling of diffusion and relaxation. Int J pharm, 1989, 57(2):169-72.
36. Esfahanian M, Ghasemzadeh MA, Razavian SMH, Synthesis, identification and application of the novel metal-organic framework $Fe_3O_4$@PAA@ZIF-8 for the drug delivery of ciprofloxacin and investigation of antibacterial activity. Artif Cells, Nanomed Biotechnol, 2019, 47(1):2024-2030.